

DOI: 10.1002/adma.200703102

## Patterned Growth and Transfer of ZnO Micro and Nanocrystals with Size and Location Control\*\*

By Jesse J. Cole, Xinyu Wang, Robert J. Knuesel, and Heiko O. Jacobs\*

ZnO micro- and nanostructures have been produced using a large number of different synthetic routes,<sup>[1]</sup> and the applications that utilize their unique properties keep increasing. The 3.3 eV direct bandgap and 60 meV exciton binding energy is exploited in ultraviolet optoelectronics,<sup>[2–4]</sup> room-temperature lasing,<sup>[5–8]</sup> and solar cells applications;<sup>[9–11]</sup> extremely long photocarrier lifetimes have been observed yielding UV photodetectors with  $10^8$  internal gain;<sup>[12]</sup> the optical properties in combination with n-type conduction support transparent transistor and display applications,<sup>[13,14]</sup> while the piezoelectricity is utilized in power generation<sup>[15]</sup> and force sensing applications.<sup>[16]</sup> The integration of these device prototypes on a wafer scale will require access to ZnO micro- and nanostructures with a variety of dimensions at known locations. A wet-chemical approach is desirable for reasons of processing cost when compared with gas-phase methods, and a number of patterned and seeded growth methods have been reported. Patterned self-assembled monolayers with hydrophobic and hydrophilic endgroups have been used on silver<sup>[17]</sup> or silicon substrates<sup>[18]</sup> yielding densely packed 400 nm diameter and 2  $\mu\text{m}$  long ZnO nanorods in regions that were 2  $\mu\text{m}$  wide with empty areas in between. Out-of-plane orientation varied but has been improved by seeding ZnO nanocrystals through thermal oxidation of zinc acetate.<sup>[19]</sup> Perfect vertical orientation, however, requires substrates such as GaN,  $\text{MgAl}_2\text{O}_4$ ,<sup>[20]</sup> or sapphire,<sup>[21]</sup> which can be partially masked with photoresist to achieve patterned growth. Qualitatively all of these methods produce nanorods in the seeded or unmasked areas with limited control over the location and density. Continued growth leads to coalescence into a polycrystalline film as the diameter increases with grain boundaries and defects in between. Continued growth in combination with photoresist has also been reported to lead to a lateral overgrowth; a previously reported concept to produce high-quality GaN thin films.<sup>[22]</sup> For ZnO on  $\text{MgAl}_2\text{O}_4$ , lateral growth over patterned photoresist improved the dislocation density by a factor of 100 compared to the window region containing coalesced nanorods.<sup>[20]</sup> Subsequent growth using a second window yielded continuous ZnO thin films with reduced dislocations.<sup>[21]</sup>

This Communication reports on a new method that uses oxygen plasma to surface-engineer nucleation areas to produce vertical single-crystal ZnO nanowire rows and extended wall structures on p-type GaN at addressable locations on a surface with tailored  $>100$  nm lateral dimensions and  $<100$  nm lateral positional accuracy. The concept uses a plasma process and photoresist patterns to reveal nonoxidized magnesium sites that nucleate growth. Nucleation in nonoxidized areas is followed by epitaxial overgrowth producing patterned areas of ZnO over 2 inch (1 inch = 2.54 cm) wafers. Adjusting pH increased ZnO deposition yield and enabled formation of high-quality ZnO crystals. Transfer printing onto a flexible substrate is also demonstrated.

Figure 1 shows the patterned growth process. Photolithography, oxygen plasma treatment, and solution-based growth are the basic process steps to produce ZnO micro and nanocrystals at exact locations on a surface. The oxygen plasma is used to oxidize Mg dopants to inhibit nucleation and growth in the center area while it etches the resist, leaving behind a transitional region to nucleate ZnO growth. Subsequent lateral epitaxial overgrowth yields ZnO structures that are larger in diameter than the initial nucleation region. A Novolac-based resist (Fig. 1A) is patterned onto a Mg-doped GaN surface (Fig. 1B) by standard photolithography, as described in the Experimental section. The patterns can directly be used for growth leading to a polycrystalline ZnO film in the exposed GaN areas, which shows that the basic developer containing sodium hydroxide and exposure to photoresist do not adversely affect ZnO nucleation on p-type GaN. However, to produce single-crystal structures of high quality a plasma treatment is required (Fig. 1C). The treatment yields a narrow nucleation region in which the oxidation state transitions from fully oxygen-passivated to partially oxidized and nonoxidized while it removes organic residues on the GaN surface, which is required to accomplish uniform growth over the entire wafer.<sup>[23]</sup> We optimized this process and exposure to a 100 Watt, 100 mTorr (1 Torr =  $1.333 \times 10^2$  Pa) oxygen plasma for 30 seconds worked best to completely prevent nucleation on fully oxygen-passivated Mg-doped GaN. The growth of ZnO (Fig. 1D) is carried out in a glass vial following a previously published procedure<sup>[17]</sup> using zinc acetate and hexamine, as described in the Experimental section. The only parameter that was modified was the initial pH. We found that the initial pH of the growth solution is an important additional parameter to control. The glass vial initially contained deionized water at pH 5.5; the slightly acidic nature is attributed to  $\text{CO}_2$  absorption from the ambient environment.

[\*] Prof. H. O. Jacobs, J. J. Cole, Dr. X. Wang, R. J. Knuesel  
University of Minnesota  
Electrical Engineering  
Rm. 4-178, 200 Union St. SE, Minneapolis, MN 55455 (USA)  
E-mail: hjacobs@umn.edu

[\*\*] We acknowledge support of this work by NSF DMI-0556161 and NSF DMI-0621137. We also acknowledge NSF MRSEC Awards DMR-0212302, ECS-0229087, ECS-0407613 for early seed support.

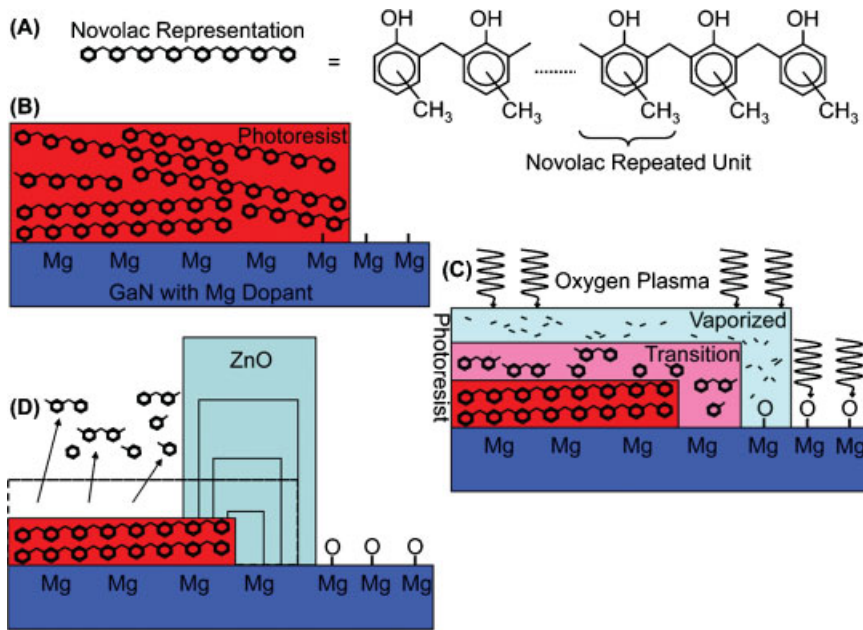


**Figure 1.** Process steps for producing ZnO crystals through nucleation at the photoresist/GaN interface. A) A conventionally patterned Novolac-based photoresist on B) Mg-doped GaN is exposed to C) an oxygen plasma to deactivate Mg dopants, which otherwise act as nucleation sites, as well as to produce a transitional region that contains nonoxidized Mg to nucleate growth. D) Solution growth at different pH values and growth times yields individual and merged laterally overgrown ZnO structures.

It was necessary to increase the initial pH to 7.5 by adding small amounts of ammonium hydroxide, NH<sub>4</sub>OH, to form continuous extended single crystals.

Figure 2 shows representative images of ZnO structures that formed at the plasma-activated interface; with an increase in pH from 5.5 to 7.5 the crystals transitioned from individual ZnO nanorods (Fig. 2A) to single-crystal lines with a rectangular 1 μm wide and 0.8 μm tall cross section (Fig. 2B). Independent of the pH, no nucleation and growth was observed on either the photoresist or the GaN that was fully oxidized. The presence of Mg dopant is the key to accomplish the observed localized nucleation in some areas and passivation in others. A number of control experiments that support this claim have been carried out. First, we were not able to produce single crystals with high dimensional control on undoped and n-doped ( $5 \times 10^{17} \text{ cm}^{-3}$  Si) GaN samples in concurrent growth experiments (90 min, 90 °C, 25 mM zinc acetate, 25 mM hexamethylenetetramine, initial pH 7.5) with p-doped ( $5 \times 10^{18} \text{ cm}^{-3}$  Mg) GaN control substrates. The undoped and n-type samples produced ZnO structures with uncontrolled nucleation sites. While we did find that ZnO could be hydrothermally grown on undoped and n-type GaN, this ZnO deposition was minimal and potentially related to surface contamination. Second, complete deactivation of the nucleation sites through oxygen plasma treatment was only observed using Mg-doped substrates. We also found that the photolithographic process was not the primary cause of the suppressed growth in exposed regions. As a control experiment we partially covered the bare p-type GaN using a glass slide to produce a partially oxidized surface using the oxygen plasma and observed that

subsequent growth revealed a 1.5 μm thick continuous polycrystalline ZnO film in the nonoxidized areas, and no ZnO in the area that was fully exposed to the plasma.

The observation of the increased nucleation in the magnesium-rich areas can be explained by looking at the electronegativity: Magnesium is an alkaline earth metal that exhibits greater ionic characteristics and lower electronegativity than the group III element gallium. Mg–O (oxygen electronegativity: 3.5) is more energetically stable than Mg–N (nitrogen electronegativity: 3.1). The enhanced ionic characteristic of magnesium within the GaN lattice should lead to an enhanced concentration and attachment of precursor ions such as OH<sup>−</sup>, Zn<sup>2+</sup>, and their complexes. The affinity of OH<sup>−</sup> and subsequent localized decomposition of Zn(OH)<sub>2</sub> is expected to lead to a preferential nucleation and growth in the Mg-rich region. Second, plasma-oxidized Mg sites should suppress OH<sup>−</sup> attachment and nucleation in areas towards the center of exposed GaN. This is consistent with the experiment and most

likely the reason of the high selectivity in the growth that we observed. The point of zero charge for bulk MgO is widely accepted as 12. This implies that MgO preferentially adsorbs H<sup>+</sup> and suppresses OH<sup>−</sup> attachment for the experimental pH range described here. Considering the MgO point of zero charge, we speculate that ZnO nucleation on oxidized Mg locations may be possible if growth pH is held above pH 12. In summary, Mg sites are active and readily oxidized. Nonoxidized Mg sites nucleate growth, whereas the formation of an ionic Mg–O bond through plasma oxidation deactivates nucleation. Once nucleation has occurred and facets are produced the ZnO growth continues independent of the substrate. In other words: the presence of the substrate is no longer relevant and growth does not deviate from conventional ZnO hydrothermal deposition. For example, HMT (hexamethylenetetramine) increases the aspect ratio but does not completely stop lateral growth. With an initial pH of 7.5 and assuming that ZnO growth occurs immediately upon immersion in the growth solution, the growth rate can be estimated at 2.8 Å s<sup>−1</sup> along the *c*-axis and 0.8 Å s<sup>−1</sup> along the *a*- or *b*-axis crystallographic direction.

Figure 3 shows a set of ZnO wall and interdigitated electrode-type structures formed using a two step lithography–oxidation sequence to illustrate that lithographic processing does not adversely affect previously oxidized nucleation sites. Oxidized areas can be formed using a sequence of sequential masking and oxidation steps yielding more complex patterns. The first sequence used photolithography, plasma oxidation, and removal of resist to produce parallel lines of fully oxidized

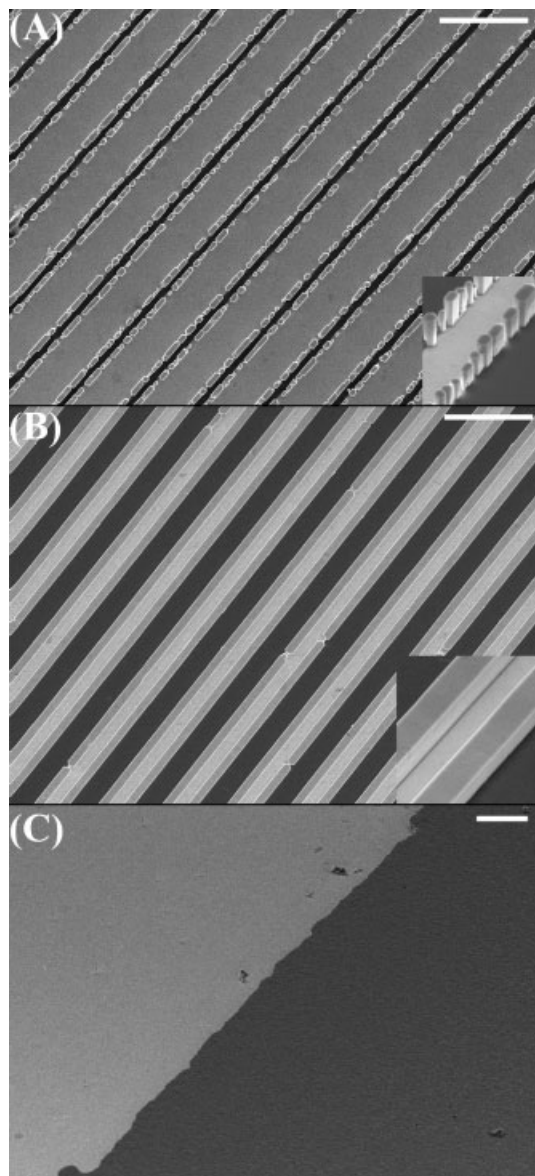


**Figure 2.** Patterned integration of ZnO structures through passivation/activation of Mg nucleation sites on GaN substrates. A) Isolated nanorods or B) extended single crystals form at the GaN-photoresist interface when the initial pH is 5.5 or 7.5, respectively. C) Control experiment depicting step edge and complete suppression of growth in oxygen plasma treated regions (light) and uniform growth in the Mg doped area (dark). 10  $\mu\text{m}$  scale bars.

GaN. Next we repeated the process whereby the photoresist pattern crosses the original pattern at controlled angles; the wall structures (Fig. 3A and B) had an angle of  $90^\circ$ , and the interdigitated electrode structures (Fig. 3C) had an angle of roughly  $1^\circ$  between the initial oxidized GaN strips and final photoresist trenches; the resist is not removed during the second step to yield narrow nucleation regions and illustrated structures.

Using the photomasks the structures can be placed with ca. 100 nm nearest-neighbor positional accuracy, calculated by

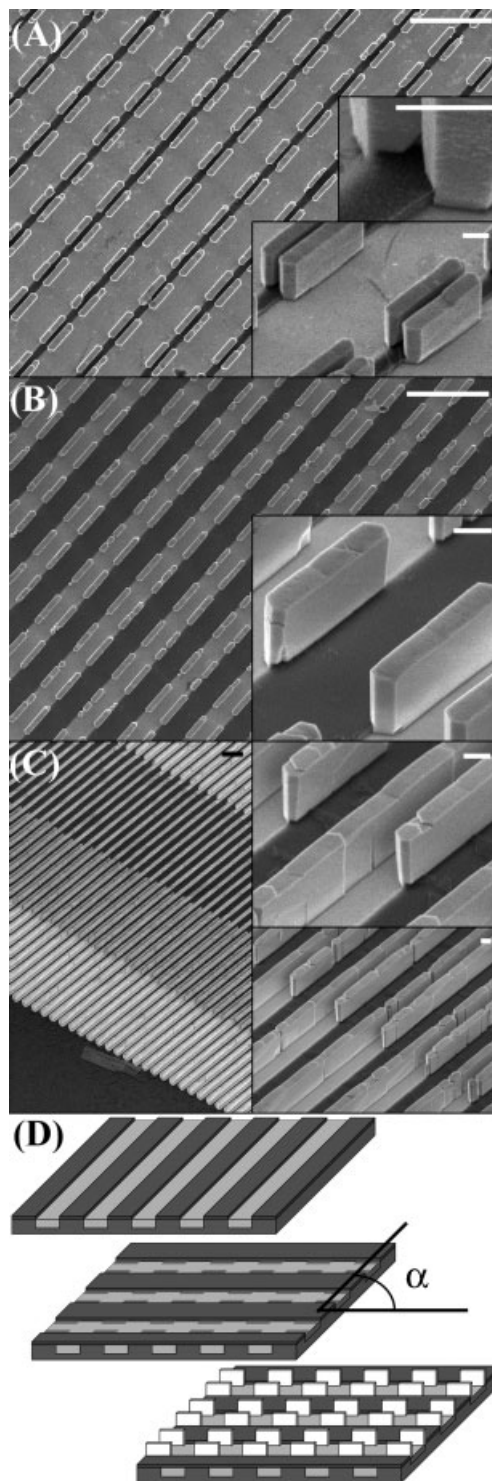


**Figure 3.** ZnO structures fabricated by multiple oxidation steps. Angle between initially oxidized GaN strips and final ZnO nucleation strips was varied from  $90^\circ$  (A,B) to approximately  $1^\circ$  (C), resulting in walls and interdigitated electrode type structures, respectively. Increasing the angle  $\alpha$  between first (D top) and second (D middle) oxidation steps decreased lengths of the resulting ZnO crystals (D bottom). 10  $\mu\text{m}$  scale bars in (A–C). 1  $\mu\text{m}$  scale bars in insets.



measuring the center-to-center distance (90 nm STD, Fig. 2B; 120 nm STD, Fig. 3A) of the ZnO crystals that have been produced. The use of higher-resolution e-beam patterns could reduce these numbers. Lateral overgrowth leads to well-defined crystals with a narrow size distribution. We measured a variation of 60 nm or smaller (5% STD) considering the lateral width perpendicular to photoresist barrier (Figs. 2B and 3A). This confinement was not as narrow using the oxide-only-barrier; walls limited to 5  $\mu\text{m}$  (Fig. 3A) in the longitudinal direction using an oxide-only-barrier varied by 80 nm (1.4% STD).

The size and area of the attachment points to GaN can be a fraction of the overall ZnO crystal size. The inset of Figure 3a shows the trunk of the produced structures; approximately 50% of the footprint sits on the photoresist in this case. This allows detachment and transfer of overgrown ZnO crystals to flexible substrates through interfacial cleavage/delamination at the ZnO/GaN interface. Figure 4 shows a first example transferring a  $10 \times 10$  array of 25  $\mu\text{m}$  long and 2  $\mu\text{m}$  wide crystals onto an epoxy thin film. We supported the ZnO structures prior transfer by spin-coating a 10  $\mu\text{m}$  thin layer of SU-8 2010 onto the structure (2500 rpm, 95  $^{\circ}\text{C}$ /120 s soft-bake, 20 s UV exposure, and 95  $^{\circ}\text{C}$ /120 s hard bake). The use of a low-viscosity SU-8 solution helped to form a conformal initial coating. Subsequently we applied a second 200  $\mu\text{m}$  thick layer (100 rpm, 95  $^{\circ}\text{C}$ /300 s soft-bake, 120 s UV exposure, and 95  $^{\circ}\text{C}$ /

1 h hard bake) to produce a film with sufficient mechanical strength. The entire epoxy film (Fig. 4A) including the ZnO can be delaminated through rapid thermal-cooling-induced stress by placing the sample on an unheated copper plate at the end of the final hard bake cycle. The film tends to curl and was further attached to a poly(ethylene terephthalate) (PET) film to characterize the flexible and optically transparent ZnO and SU-8 composite structure (Fig. 4B–D).

The reported nucleation and growth process provides a new route towards the production of ZnO micro- and nanostructures at known locations (ca. 100 nm STD) with well-defined dimensions (as low as 1.4% STD). The resulting structures are attractive for a number of applications that aim at integrating ZnO devices such as ultraviolet LEDs,<sup>[2–4]</sup> laser cavities,<sup>[24]</sup> waveguides,<sup>[5–8]</sup> high-gain photodetectors,<sup>[12]</sup> solar cells,<sup>[9–11]</sup> sensors, piezoelectric actuators<sup>[16]</sup> or micro-power generators<sup>[15]</sup> at exact known locations. A first step towards the transfer of the structures onto flexible substrates has been made. Measurements of the electrical and optical properties are underway and will be published elsewhere.

## Experimental

**Photoresist Patterning:** Mg-doped GaN was used as a substrate, with doping concentration  $5 \times 10^{18} \text{ cm}^{-3}$  (TDI inc., Silver Spring, MD). The substrate was photolithographically patterned conventionally. Following a dehydration prebake at 115  $^{\circ}\text{C}$  for 60 seconds, Shipley 1805 photoresist was spun at 3000 rpm, soft-baked at 105  $^{\circ}\text{C}$  for 60 seconds, exposed using a Karl Suss MA-6 Mask Aligner, and developed in Microposit 351 developer for 30 seconds. Shipley 1805 is a Novolac-based photoresist that can require descum processing after patterning. The only descum process used here was exposure to the oxygen plasma, which also provided a means for ZnO nucleation control.

**ZnO Crystal Synthesis:** The ZnO growth solution was prepared by adding zinc acetate,  $\text{Zn}(\text{CH}_3\text{COO})_2$ , and hexamethylenetetramine,  $(\text{CH}_2)_6\text{N}_4$ , to 70 mL of deionized water such that the solution contained 25 mM of each compound. The pH was adjusted by adding ammonium hydroxide,  $\text{NH}_4\text{OH}$ , to the initially acidic solution and checked in real time with an electronic pH probe. The probe was removed to prevent unwanted pH probe electrolyte solution from leaking into the growth solution. Patterned and oxidized GaN samples were inserted into the growth solution. To grow the ZnO crystals, the solution was heated in an oven to 90  $^{\circ}\text{C}$  for times ranging between 10 min to 3 h. GaN samples were held in the growth solution with glass slides, because metal clips were corroded by the growth solution, reducing uniformity in ZnO deposition. Following the growth, samples were removed from solution and briefly rinsed with DI water.

Received: December 13, 2007

Revised: January 18, 2008

Published online: April 1, 2008

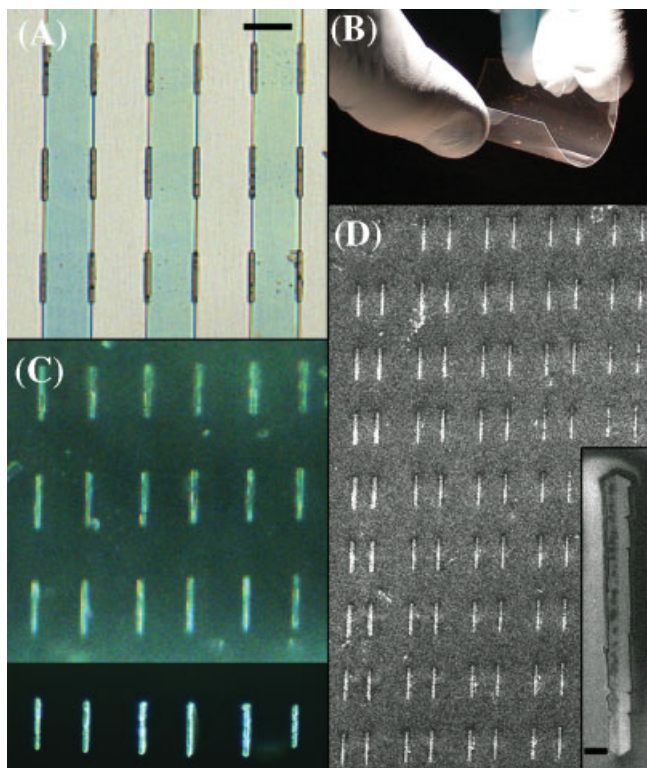


**Figure 4.** ZnO transfer to a flexible substrate. Fabricated ZnO prior (A) and after transfer (B–D) onto a 200  $\mu\text{m}$  thick epoxy-PET flexible substrate. Dark field (C), fluorescence (C, inset), and SEM (D) micrographs of ZnO epoxy composite structure after transfer. 25  $\mu\text{m}$  scale bar in (A). 2  $\mu\text{m}$  scale bar in (D inset).

- [1] Z. Fan, J. G. Lu, *J. Nanosci. Nanotechnol.* **2005**, *5*, 1561.
- [2] R. D. Vispute, V. Talyansky, S. Choopun, R. P. Sharma, T. Venkatesan, M. He, X. Tang, J. B. Halpern, M. G. Spencer, Y. X. Li, L. G. Salamanca-Riba, A. A. Iliadis, K. A. Jones, *Appl. Phys. Lett.* **1998**, *73*, 348.
- [3] X. Wang, J. Cole, A. M. Dabiran, H. O. Jacobs, *Mater. Res. Soc. Symp. Proc.* **2007**, *1018*, 8.

- [4] X. Wang, J. Cole, H. O. Jacobs, *Proc. 2007 NSTI Nanotechnology Conf.*, vol.4, Nano Science and Technology Institute, Danville, CA **2007**, p. 562.
- [5] P. Yang, H. Yan, S. Mao, R. Russo, J. Johnson, R. Saykally, N. Morris, J. Pham, R. He, H.-J. Choi, *Adv. Funct. Mater.* **2002**, *12*, 323.
- [6] H. Yan, J. Johnson, M. Law, R. He, K. Knutsen, J. R. McKinney, J. Pham, R. Saykally, P. Yang, *Adv. Mater.* **2003**, *15*, 1907.
- [7] R. Hauschild, H. Kalt, *Appl. Phys. Lett.* **2006**, *89*, 123107/1.
- [8] L. K. van Vugt, S. Ruehle, D. Vanmaekelbergh, *Nano Lett.* **2006**, *6*, 2707.
- [9] M. Law, E. Greene Lori, C. Johnson Justin, R. Saykally, P. Yang, *Nat. Mater.* **2005**, *4*, 455.
- [10] K. S. Leschkies, R. Divakar, J. Basu, E. Enache-Pommer, J. E. Boercker, C. B. Carter, U. R. Kortshagen, D. J. Norris, E. S. Aydil, *Nano Lett.* **2007**, *7*, 1793.
- [11] C. Levy-Clement, R. Tena-Zaera, M. A. Ryan, A. Katty, G. Hodes, *Adv. Mater.* **2005**, *17*, 1512.
- [12] C. Soci, A. Zhang, B. Xiang, S. A. Dayeh, D. P. R. Aplin, J. Park, X. Y. Bao, Y. H. Lo, D. Wang, *Nano Lett.* **2007**, *7*, 1003.
- [13] S. Ju, K. Lee, D. B. Janes, M.-H. Yoon, A. Facchetti, T. J. Marks, *Nano Lett.* **2005**, *5*, 2281.
- [14] M. Futua, H. Furuta, T. Matsuda, T. Hirao, T. Hiramatsu, H. Hokari, M. Yoshida, *Mater. Integr.* **2006**, *19*, 10.
- [15] J. Schrier, D. O. Demchenko, L.-W. Wang, A. P. Alivisatos, *Nano Lett.* **2007**, *7*, 2377.
- [16] X. Wang, J. Zhou, J. Song, J. Liu, N. Xu, Z. L. Wang, *Nano Lett.* **2006**, *6*, 2768.
- [17] J. W. P. Hsu, Z. R. Tian, N. C. Simmons, C. M. Matzke, J. A. Voigt, J. Liu, *Nano Lett.* **2005**, *5*, 83.
- [18] Y. Masuda, N. Kinoshita, F. Sato, K. Koumoto, *Cryst. Growth Des.* **2006**, *6*, 75.
- [19] L. E. Greene, M. Law, D. H. Tan, M. Montano, J. Goldberger, G. Somorjai, P. Yang, *Nano Lett.* **2005**, *5*, 1231.
- [20] D. Andeen, J. H. Kim, F. F. Lange, G. K. L. Goh, S. Tripathy, *Adv. Funct. Mater.* **2006**, *16*, 799.
- [21] J. H. Kim, D. Andeen, F. F. Lange, *Adv. Mater.* **2006**, *18*, 2453.
- [22] S. Nakamura, M. Senoh, S.-i. Nagahama, N. Iwasa, T. Yamada, T. Matsushita, H. Kiyoku, Y. Sugimoto, T. Kozaki, H. Umemoto, M. Sano, K. Chocho, *Appl. Phys. Lett.* **1998**, *72*, 211.
- [23] Additional transition region information: The transitional region consists of a gradient of Mg dopand sites which were partially shielded from the oxidative effects of the plasma, yet permits ZnO to deposit in solution. The oxygen plasma etching of photoresist is widely used in industry and has been successfully modeled by the Hougen–Watson method as the ion-assisted chemical etch of Novolac polymer chains by oxygen radicals [25]. Oxygen radicals impact and react with the photoresist to break covalent C–C bonds (3.6 eV per bond) to separate the original polymer chains and/or remove some material as volatile products such as CO<sub>x</sub> and H<sub>2</sub>. Oxygen plasma etching results from breakage of carbon bonds responsible for chain cohesion, then atomization of shortened chain constituents to expose unreacted long photoresist chains below. The process can be interrupted, which leaves a transitional region that includes a photoresist layer with shortened polymer chains and substrate surface region that transitions from “no” to “full” oxygen plasma exposure. We have conducted oxygen plasma etching experiments which support the model. Photoresist was patterned on a substrate, then half of the substrate was covered with a glass slide. The substrate was exposed to oxygen plasma, such that slide-covered areas were protected from plasma exposure. Exposure to oxygen plasma was found to cause lateral etching of the photoresist. The lateral photoresist etch rate was experimentally determined as 125 nm min<sup>-1</sup>. The reaction time required to vaporize the photoresist implies that a sub-100 nm transition region forms at the point where photoresist chains transition from initial polymer chain length to shortened volatile hydrocarbons.
- [24] M. H. Huang, S. Mao, H. Feick, H. Yan, Y. Wu, H. Kind, E. Weber, R. Russo, P. Yang, *Science* **2001**, *292*, 1897.
- [25] R. P. Bray, R. R. Rhinehart, *Plasma Chem. Plasma Process.* **2001**, *21*, 149.